ELSEVIER

Journal of Power Sources 83 (1999) 170–177

JOURNAL OF POWER SOURCES

www.elsevier.com/locate/jpowsour

Ni-SDC cermet anode for medium-temperature solid oxide fuel cell with lanthanum gallate electrolyte

Xinge Zhang [a,*], Satoshi Ohara [a], Radenka Maric [a], Kazuo Mukai [a], Takehisa Fukui [a], Hiroyuki Yoshida [b], Masayoshi Nishimura [b], Toru Inagaki [b], Kazuhiro Miura [c]

[a] *Japan Fine Ceramics Center, 2-4-1 Mutsuo, Atsuta-ku, Nagoya 456-8587, Japan*
[b] *Kansai Electric Power, 11-20 Nakoji 3-chome, Amagasaki, Hyogo-ken 661-0974, Japan*
[c] *Kanden Kakou, 3-95 Showa-dori, Amagasaki, Hyogo-ken 661-0881, Japan*

Received 6 April 1999; accepted 21 April 1999

Abstract

The polarization properties and microstructure of Ni-SDC (samaria-doped ceria) cermet anodes prepared from spray pyrolysis (SP) composite powder, and element interface diffusion between the anode and a $La_{0.9}Sr_{0.1}Ga_{0.8}Mg_{0.2}O_{3-\delta}$ (LSGM) electrolyte are investigated as a function of anode sintering temperature. The anode sintered at 1250°C displays minimum anode polarization (with anode ohmic loss), while the anode prepared at 1300°C has the best electrochemical overpotential, viz., 27 mV at 300 mA cm^{-2} operating at 800°C. The anode ohmic loss gradually increases with increase in the sintering temperature at levels below 1300°C, and sharply increases at 1350°C. Electron micrographs show a clear grain growth at sintering temperatures higher than 1300°C. The anode microstructure appears to be optimized at 1300°C, in which nickel particles form a network with well-connected SDC particles finely distributed over the surfaces of the nickel particles. The anode sintered at 1350°C has severe grain growth and an apparent interface diffusion of nickel from the anode to the electrolyte. The nickel interface diffusion is assumed to be the main reason for the increment in ohmic loss, and the resulting loss in anode performance. The findings suggest that sintering Ni-SDC composite powder near 1250°C is the best method to prepare the anode on a LSGM electrolyte.

Keywords: Ni-SDC anode; Sintering temperature; LSGM; SOFC

1. Introduction

In order to realize a practical solid oxide fuel cell (SOFC) which operates at medium temperature (800°C or less), it is essential to develop an electrolyte and electrodes with high performance. Recently, $LaGaO_3$-based perovskite oxides have been proposed [1–6] as possible electrolyte materials. Among these oxides, $La_{0.9}Sr_{0.1}Ga_{0.8}Mg_{0.2}O_{3-\delta}$ (abbreviated as LSGM) demonstrates a high oxygen ion conductivity of about 0.10 S cm^{-1} at 800°C, i.e., four times higher than that of yttria stabilized zirconia (YSZ) which is the conventional electrolyte used in SOFCs. LSGM also possesses negligible electronic conduction at temperatures below 1000°C over a broad range of oxygen partial pressures from pure oxygen ($p_{O_2} = 0.1$ MPa) to moistened hydrogen ($p_{O_2} \sim 10^{-21}$ MPa), and a relatively good chemical stability [7] and mechanical strength [8].

In the search of high performance electrodes, doped ceria, particularly samaria-doped ceria (SDC), has been examined [4–13] as an anode material. In fact, SDC has also been studied as an electrolyte. The oxygen ion conductivity of SDC is almost the same as LSGM [10,11]. SDC also has a high electronic conduction in reducing atmosphere (> 0.2 S cm^{-1} at 800°C) because the reduction of the ceria oxide produces oxide ion vacancies and free electrons in the solid [10–12]. Use of SDC as anode material is expected to yield high performance given that the mixed conductivity of ceria-based oxide results in an enlargement of the reaction zone to include the entire particle surface beyond the boundary zone of the physical contact points between the anode and the electrolyte.

Ceria-based anodes can be grouped into three types: (i) doped ceria anodes without any metal component [14–20]; (ii) doped ceria anodes with highly dispersed metal cata-

* Corresponding author. Tel.: +81-528713491; fax: +81-528713599; E-mail: zhang@jfcc.or.jp

0378-7753/99/$ - see front matter
PII: S0378-7753(99)00293-1

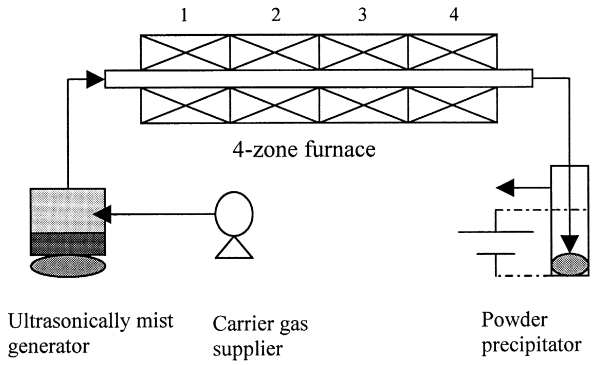

Fig. 1. Schematic diagram of SP system.

lysts [9,12,13,17,21]; (iii) nickel and doped (or undoped) ceria cermet anodes [5,22,23]. Among these, the highest performance has been obtained for type (ii) materials. The improvement in the anode performance by dispersed nanometer-size electroactive microcatalysts (such as Ru, Rh, Ir, Pd, and Pt) indicates that the less active sites on the SDC are modified by the microcatalysts to form more active sites at the boundary between the noble metal-catalyst, the SDC and H_2.

The activity and stability of an electrode depend not only on the chemical composition, but also on the microstructure. The latter is closely related to the powder preparation and the electrode fabrication. Previous studies on the long-term stability of a Ni-YSZ cermet anode [24,25] and the high performance of a $LaSrMnO_3$–YSZ composite cathode [26,27] have demonstrated the importance of microstructure control in obtaining a good electrode performance. A recent study [28] on the high-performance Ni-SDC cermet anode using YSZ as an electrolyte for medium operation temperature has also indicated the strong influence of sintering temperature on anode performance through effecting a change in the microstructure [28].

The influence of the sintering temperature (T_s) of a Ni-SDC anode on its performance with LSGM as a electrolyte is the aim of this study. In particular, an attempt is made to find an optimized microstructure for a high-performance Ni-SDC cermet anode in LSGM electrolyte. Based on previous research on a YSZ electrolyte [28], four sintering temperatures (1200, 1250, 1300, and 1350°C) are selected. Electrochemical measurement and surface analysis techniques are used to understand the effect of sintering temperature on the microstructure and performance of a Ni-SDC cermet anode.

2. Experimental

2.1. Ni-SDC composite powder preparation

SDC of chemical composition $(CeO_2)_{0.8}(SmO_{1.5})_{0.2}$ was used in this investigation because it displays the highest ionic conductivity among the rare-earth-oxides-doped ceria conductors, viz., 0.0945 S cm^{-1} at 800°C [10]. Ni-SDC composite powder with a typical composition Ni:SDC = 1:1 (vol.%) was prepared by a spray pyrolysis (SP) technique [26–28]. A schematic diagram of the SP system is presented in Fig. 1. This system consists of a carrier gas supplier (air is generally used as the carrier gas), a solution chamber with ultrasonic vibrators for mist generation, a furnace with a four-temperature zone for reaction and calcination, and an electrostatic precipitator for powder collection. The experimental conditions of the SP technique, the composition of the starting solution and the properties of the prepared powder are listed in Table 1.

$La_{0.6}Sr_{0.4}CoO_{3-\delta}$ (LSCo) powder was also prepared by a SP technique and served as the standard cathode material in this study.

After SP preparation, both Ni-SDC and LSCo composite powders were further calcinated at 1000°C in air for 24 h.

2.2. Single cell construction

An anode–electrolyte–cathode assembly was prepared on a $La_{0.9}Sr_{0.1}Ga_{0.8}Mg_{0.2}O_{3-\delta}$ (LSGM) electrolyte (diameter = 14 mm; thickness = 500 μm). The thickness of the LSGM electrolyte was controlled precisely by grinding down a sintered (1500°C; 10 h) thick pellet with a diamond wheel. Polyethylene glycol (PEG) was used as a binder to prepare the electrode paste for screen printing the anode and the cathode. The weight ratio of electrode composite powder to PEG was 2.5:1, both in the anode and in the cathode. The anode was first printed and sintered in air for 2 h at 1200, 1250, 1300 or 1350°C,

Table 1
Composition, SP conditions and properties of prepared Ni-SDC composite powder

Composition of starting solution		SP conditions		Properties of composite powder	
$Ni(CH_3COO)_2$ (mol dm^{-3})	0.05	Temperature profile (°C)	200 (1)[a] 400 (2) 800 (3) 1000 (4)	Particle morphology	Regular sphere [28,33]
$Sm(NO_3)_3$ (mol dm^{-3})	0.01	Air flow-rate (l min^{-1})	3	Mean particle size (μm)	~ 0.5
$Ce(NO_3)_4$ (mol dm^{-3})	0.04	Frequency (MHz)	1.7	Specific area (m^2 g^{-1})	> 2

[a] Temperatures controlled in four-zone furnace (see Fig. 1).

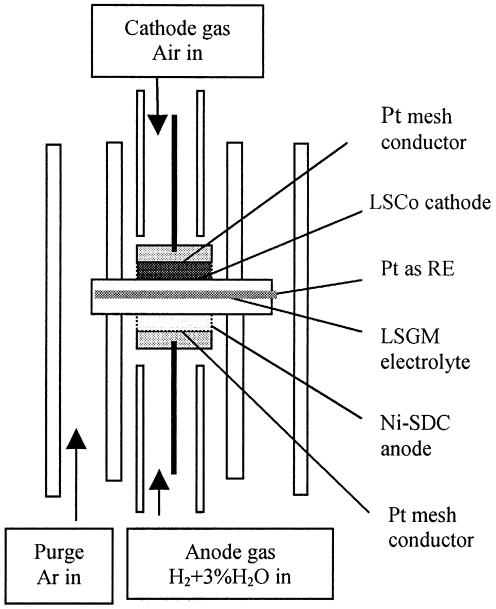

Fig. 2. Schematic diagram of single-cell test.

respectively. Then, a LSCo cathode was printed on the opposite surface and sintered at 1000°C in air for 4 h. In order to measure the electrode polarization, a piece of platinum wire (diameter = 0.3 mm) was wound around the LSGM electrolyte pellet, fixed with platinum paste, and sintered at 800°C in air for 2 h. A soft-glass ring was used as a sealing gasket to avoid leakage of the reactant gases. The assembled cell was placed in the hot zone of a vertical furnace. The cell configuration is shown in Fig. 2. The temperature was first increased to 900°C at a rate of 300°C h^{-1} kept at this value for 10 min for good glass sealing, and then decreased to 800°C, i.e., the operation temperature of the cell. Air was supplied directly to the cathode side at a flow rate of 50 ml min^{-1}, while water-moistened (at 25°C) H_2 was fed to the anode side at the same flow rate. Pure argon gas was used as a purge gas during the start-up and shut-down of the cell. The platinum reference electrode operated in pure argon atmosphere during the test. Steady-state polarization via a current-interrupt method was implemented to investigate the cell performance and the electrode polarization properties. Scanning electron microscopic (Hitachi, S-800) studies were made both on the surface and on the cross-section of the anode with LSGM electrolyte after current-interruption measurement of the cell. Element analysis was also performed by EDAX (Philips, PV9900) to investigate element inter-diffusion across the interface.

3. Results and discussion

3.1. Anode polarization properties

In this paper, the anode polarization (P_a) is defined as the potential difference between the anode and the reference electrode, which is including the electrochemical overpotential (η_a) and the ohmic loss (IR_a) between anode and the reference electrode, i.e.,

$$P_a = \eta_a + IR_a \quad (1)$$

The influences of anode sintering temperature (T_s) on P_a, η_a and IR_a is shown in Figs. 3–5, respectively. These results clearly indicate that the anode polarization depends strongly on the sintering temperature. The minimum P_a is obtained for an anode sintered at 1250°C (see Fig. 3); while the lowest η_a appears for the anode sintered at 1300°C (see Fig. 4). IR_a gradually increases with increase in T_s, and exhibits a sharp increase at 1350°C (Fig. 5).

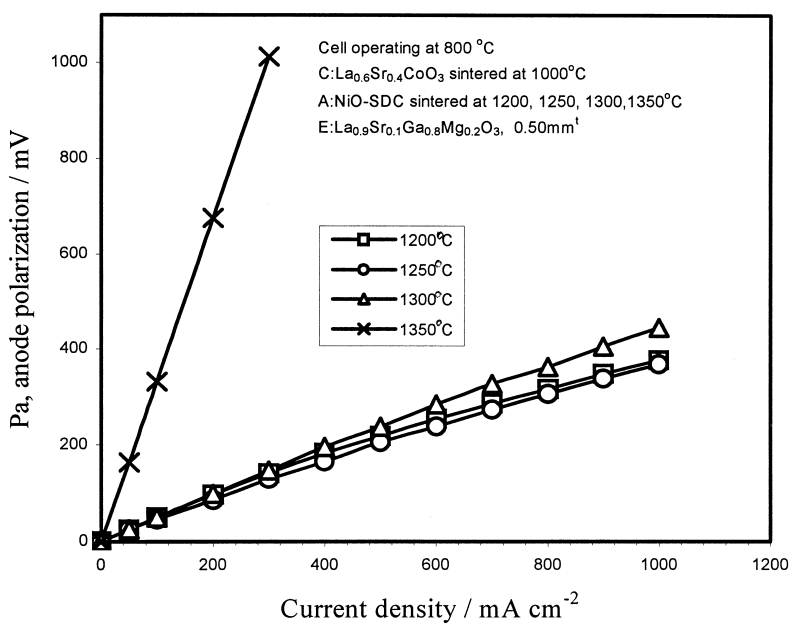

Fig. 3. Influence of sintering temperature on Ni-SDC anode polarization (with ohmic loss).

Although η_a decreases with increase in T_s from 1200 to 1300°C, there is only a small improvement in P_a between the two anodes sintered at 1250 and 1200°C. By contrast, a further increase in T_s to 1300°C increases the P_a value, especially at high current density. Remarkably, the anode sintered at 1350°C displays the worst performance, viz., a P_a value of over 1000 mV even at only 300 mA cm^{-2}. The measured η_a and IR_a values for anodes sintered at 1200, 1250, 1300, and 1350°C at a current density of 300 mA cm^{-2} are shown in Fig. 5. It appears that the improved electrochemical performance with increase in sintering temperature is counterbalanced by the corresponding increase in IR_a.

The relationship of η_a with current density (i) is described by the Tafel Eq. (2):

$$\eta_a = (RT/\alpha nF)\ln i - (RT/\alpha nF)\ln i_o \quad (2)$$

where α is the electron transfer coefficient for the H_2 oxidation reaction at the anode, and i_o is the exchange current density. From the Tafel plot (Fig. 4), the i_o value (given by the extrapolated intercept at $\eta_a = 0$) and the αn value (from the slope) can be calculated. The i_o and αn values of Ni-SDC anodes at different T_s are listed in Table 2. The i_o values are almost identical, i.e., about 150 mA cm^{-2} for $T_s \leq 1300$°C; while i_o falls to near 40 mA cm^{-2} at $T_s = 1350$°C. The value of i_o depends on the amount of reaction area and the activity of the materials. The fall in i_o can be regarded as a reflection of a great loss of reaction sites for the anode at $T_s = 1350$°C since the same anode material is used in the test. It is noticed that αn values obtained from the Tafel slope in Fig. 4 are greater than 1. Similar results have also been reported by Kawada et al. [29] and Aaberg et al. [30], even in Ni-YSZ cells. The different αn values of the anodes sintered at different T_s may suggest that the reaction mechanism and the rate-determining step (rds) vary with the anode microstructure.

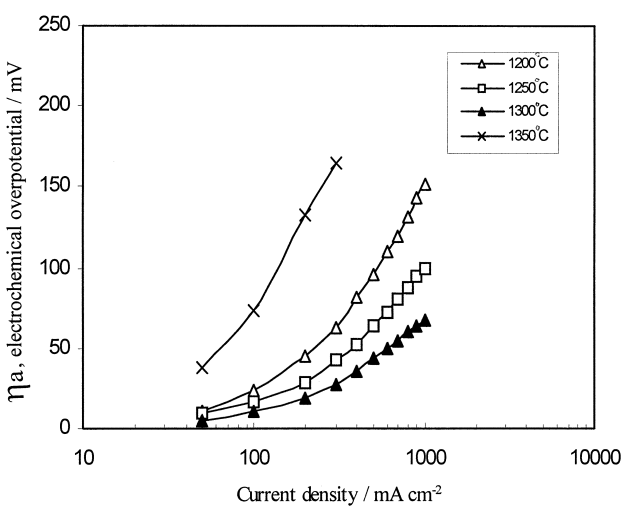

Fig. 4. Electrochemical overpotential (η_a) of Ni-SDC anodes sintered on LSGM electrolyte at different sintering temperatures.

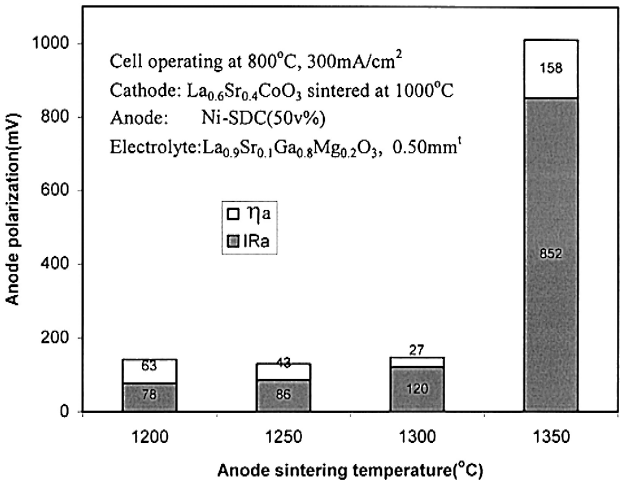

Fig. 5. Ohmic loss and electrochemical overpotential of Ni-SDC anode sintered on LSGM electrolyte at different sintering temperatures.

Referring to the simplified reaction mechanism presented by Aaberg et al. [30] for Ni-YSZ anode and considering the role of the SDC mixed conductor, we propose the following possible H_2 oxidation processes at the Ni-SDC anode:Step 1:

$$H_{2(g)} \rightarrow 2H_{ads,Ni} \quad (3a)$$

$$H_{2(g)} \rightarrow 2H_{ads,SDC} \quad (3b)$$

Step 2:

$$H_{ads,Ni} \rightarrow H^{\cdot}_{ads,SDC\,or\,LSGM} + e^{-}_{Ni} \quad (4a)$$

$$H_{ads,SDC} \rightarrow H^{\cdot}_{ads,SDC\,or\,LSGM} + e^{-}_{SDC} \quad (4b)$$

Step 3:

$$e^{-}_{SDC} \rightarrow e^{-}_{Ni} \quad (5)$$

Step 4:

$$O_{o,LSGM} \rightarrow O_{o,SDC}\,(rds) \quad (6)$$

Step 5:

$$2H^{\cdot}_{ads,SDC\,or\,LSGM} + O_{o,SDC\,or\,LSGM} \rightarrow H_2O + V_o^{\cdot\cdot}\,(rds) \quad (7)$$

Step 1 is the adsorption and dissociation of gaseous H_2 on the nickel particles and the SDC particles. According to Skaarup et al. [31], the adsorption and mobility of hydrogen on nickel is fast. Consequently, it is concluded that

Table 2
i_o and α values of Ni-SDC anodes at different T_s (from Fig. 4)

T_s (°C)	1200	1250	1300	1350
i_o (mA cm^{-2})	148	150	154	38
αn	1.20	1.82	2.66	1.18

adsorbed hydrogen atoms are abundantly present on the Ni-SDC composite particles and at the Ni/SDC/LSGM interfaces, even when the anode is moderately polarized. Step 2 is the electrochemical transfer of adsorbed hydrogen atoms to protons, including the transport of protons or hydrogen atoms from the metal to the electrolyte surface, which is the potential-dependent step and is regarded as a fast step [30,32]. Step 3 is the transfer of electrons from SDC particles (a relatively low electron conductor) to some adjacent nickel particles (a high electron conductor), which happens instantly after Step 2 because of the existence of a high conductive network of nickel particles in the anode layer [28]. Step 4 is the transport of O^{2-} from the LSGM electrolyte to the SDC particles in the anode layer. Since SDC has high oxide ion conductivity (~ 0.1 S cm^{-1} at 800°C) [10], the transfer rate depends on the contact area between the SDC particles and the LSGM electrolyte, which is affected by the SDC content in the Ni-SDC cermet anode and by its microstructure. Step 5 is the combination of protons and oxide ions on the electrolyte surface. In the case of a Ni-YSZ anode for a YSZ-based SOFC, Step 5 is regarded as the rds because of the insufficient supply of oxide ions from the YSZ [30]. Since the ion conductivity of LSGM at 800°C is the same as that of YSZ at 1000°C, it is reasonable to assume that Step 5 is the main rds in this study.

It is clear that Step 2 cannot be the main rds under the present test conditions. For if the rds was Step 2, then $n = 1$, and the calculated α values for 1300°C would be higher than 2.6 (see Table 2). In theory, however, the α value should be between 0 and 1.

To our knowledge, Steps 4 and 5 play important roles in the Ni-SDC anode performance at medium temperature (800°C) when the Ni-SDC anode is properly sintered (e.g., T_s at 1200 to 1300°C in this study). As pointed by Watanabe et al. [32], the anode performance is controlled by the rate of O^{2-} supply to the anode layer via the electrolyte, as the anode reaction rate becomes sufficiently high.

3.2. Microstructures of Ni-SDC anodes

To determine the relation between the microstructure and the anode performance, electron micrographs were taken of the surfaces of the examined Ni-SDC anodes. The morphologies of these anodes are shown in Fig. 6. The morphology of the anode sintered at 1250°C is similar to that of the anode sintered at 1200°C. The agglomerated particles of these two anodes display equiaxial and loosely sintered grains which are quite similar to the morphology of the starting powder [28]. The tendency for particle sintering developed quickly as the T_s was taken above 1300°C. The Ni-SDC composite powders have an agglomerated appearance at 1350°C. With increase in T_s, the size of the agglomerated particles of Ni-SDC increases, i.e., nearly 0.5 to 1 μm (1200 to 1250°C), 2 to 3 μm (1300°C), and > 5 μm (1350°C).

Generally speaking, a fine particle size and a large degree of porosity in the anode are required so as to allow the fuel gas to pass effectively, and to increase the reaction area of the triple phase boundary (TPB) where the oxygen ion from the electrolyte reacts with the fuel gas (H_2). For a Ni-SDC anode, the distribution and the connection between nickel and SDC fine particles are also of great importance, because the function of these two types of particles is different. Similar to the role of noble metal microcatalysts in a type (ii) ceria-based anode, the micro-nickel particles in the Ni-SDC anode are regarded as the main electrocatalytic sites for the H_2 oxidation reaction, while the SDC particles serve as the main supplier of O^{2-} besides the latter's partial role in H_2 oxidation. Therefore, nickel particles are required: (i) to be connected with the O^{2-} supplier, i.e., the network of SDC particles well linked with the LSGM electrolyte; (ii) to be connected with each other for good electron transfer for compensating the relatively low electron conductivity of SDC; (iii) to be exposed to gaseous H_2 for effective electrochemical oxidation. In our previous studies [28,33], it was observed that the nickel particles are close packed and surrounded with dense shells of small SDC particles in the starting powder prepared by SP. As shown in Fig. 6(a) and (b), the loosely packed Ni-SDC composite particles of the anodes at T_s lower than 1250°C suggests the possibility of insufficient connections both between individual particles in the anode layer and between the anode and the LSGM electrolyte. As a result, O^{2-} supply, electron transfer and effective reaction sites may all be affected by insufficient particle connections and by the detrimental structure of nickel surrounded by SDC. Therefore, a slightly higher η_a was obtained at a relatively lower T_s (1200, 1250°C). Increase in T_s causes an improvement in the connections between individual particles and between the anode layer and the LSGM electrolyte, and some nickel may slip through the SDC particle shells to provide more effective reaction sites. This results in an increase in electrochemical performance of the anode. With further increase in T_s, however, the porosity and the particle size of the anode decrease and increase, respectively. Heavily sintered grains and a great lost in porosity can lead to a decrease in anode performance, because either effect decreases the area of the TPB. This explains the increase in the electrochemical overpotential at higher T_s (1350°C). The combined effects of T_s produce a minimum value of η_a. As shown in Fig. 5, the measured η_a values display a minimum for the anode sintered at 1300°C, viz., 27 mV at 300 mA cm^{-2}. A similar dependence of η_a on T_s has been found in our previous study of a Ni-SDC anode with a YSZ electrolyte [28]. It appears that the highest performance at 1300°C is due to optimization of anode microstructure, in which nickel particles form a skeleton with the well-connected SDC particles which are finely distributed over the sur-

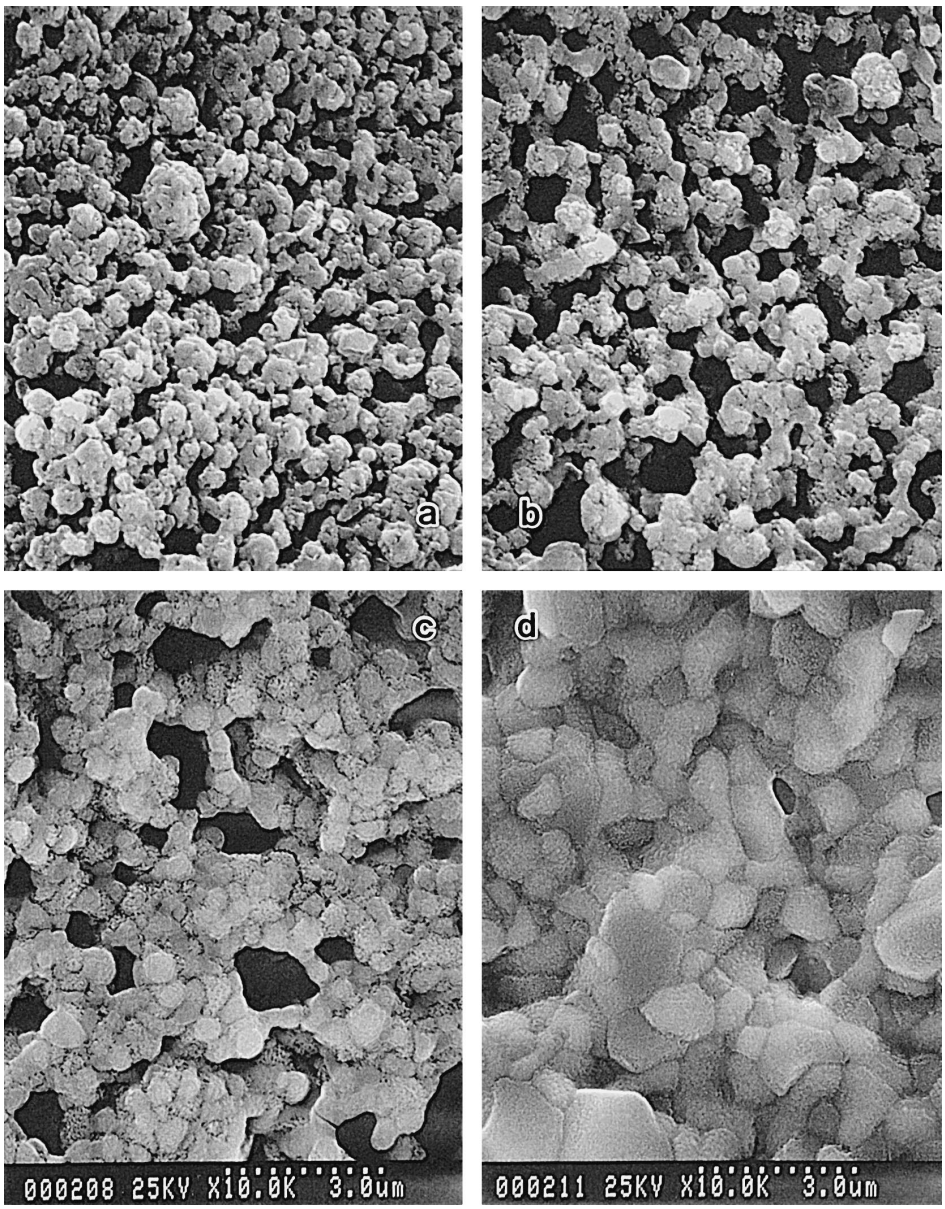

Fig. 6. Electron micrographs of Ni-SDC anode surfaces at different sintering temperatures: (a) 1200°C, (b) 1250°C, (c) 1300°C, (d) 1350°C.

faces of the nickel surfaces. The well-connected SDC microparticles form dispersed ionic paths without blocking the electronic paths of the nickel catalyst particles.

3.3. Ni interface diffusion

The anode sintered at 1300°C demonstrates the lowest η_a value due to an optimized microstructure, but its anode polarization (P_a) is higher than the anode sintered at 1250°C and even higher than the anode sintered at 1200°C (see Fig. 3). This is because of the increase in the ohmic loss with the increase of T_s (see Fig. 5). The increase in the ohmic loss indicates the possible solid reaction or element diffusion between anode and electrolyte.

In this study, the diffusion of nickel from the Ni-SDC anode into the LSGM has been observed by EDAX analysis. We found that nickel diffusion becomes more severe with increase in T_s. As shown in Fig. 7, the diffusion depth of nickel into the LSGM electrolyte is more than 5 μm at 1350°C, while little nickel diffusion could be detected at 1250°C at the LSGM surface even close to the anode side (see Fig. 7(c) and (d)). Since no other element diffusion is obvious compared with the diffusion of nickel, we attribute the increase in the ohmic loss with the increase in T_s to the diffusion of nickel. The reaction between nickel and LSGM is assumed to be the main reason by other researchers [4,5]. Huang et al. [5] reported that $LaNiO_3$ was detected (by XRD) in a LSGM + NiO mixture after co-firing at 1400°C. After firing at 1200°C, however, none of this

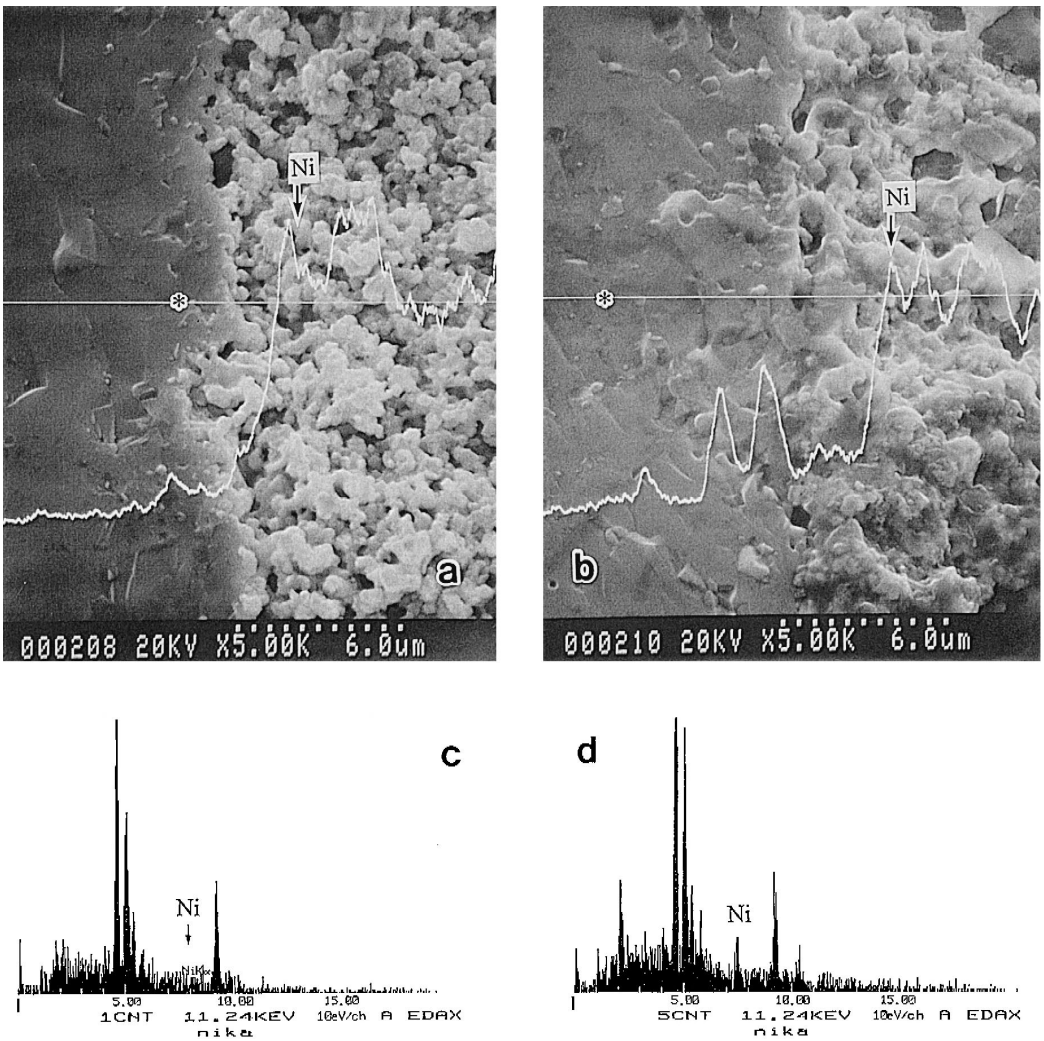

Fig. 7. EDAX analysis of nickel distribution across the interface of Ni-SDC/LSGM (upper photos). EDAX analysis of Ni, La, Ce, Ga, etc. at the (*) marked position (lower figures). (a) 1250°C, (b) 1350°C, (c) 1250°C, (d) 1350°C.

compound appeared. They supposed that the insulating lanthanum-nickel oxide would also be produced when a high current was passed through a LSGM/Ni anode interface, even at low temperature. The onset of diffusion of nickel from the anode to the LSGM electrolyte is considered to be the main cause of degradation in cell performance of a LSGM-electrolyte based cell in long-term operation [5].

There are two nickel peaks in the nickel distribution pattern across the interface between the anode sintered at 1350°C and the LSGM electrolyte (Fig. 7(b)). The reason for this may be as follows. The peak inside the LSGM may be that formed during the anode fabrication process. During the cell measurement, the previously formed Ni-rich layer electro-migrated to the inside of the LSGM by nickel ion diffusion towards the cathode under the internal electric field in the LSGM. Because of the resistance of the first formed Ni-rich layer, an extra-high temperature may be generated at the interface between the Ni-SDC anode and the LSGM electrolyte during the performance measurement. As a result, additional nickel diffusion could occur, and a second nickel peak would appear near the interface. This process is similar to the on-site diffusion of nickel at high operating current.

From the above results and discussion, it is clear that optimization of the anode sintering temperature is important to obtain a suitable microstructure and to avoid element diffusion at the interface for a high performance Ni-SDC anode prepared from SP composite powder. The increase in the IR_a loss is about six times higher than that of η_a for the anode sintered at 1350°C. Therefore, it seems quite inappropriate to prepared a Ni-SDC anode on LSGM at a T_s above this value. Because of the interface diffusion or reaction, we suggest that the optimized anode sintering temperature for a Ni-SDC cermet anode on LSGM should be a little lower than that on YSZ determined in our previous study [28].

Finally, it should be pointed out that in the investigation of electrode performance on LSGM electrolyte, reference to the value of the electrochemical overpotential (η_a) to

select the best fabrication condition is neither sufficient nor dependable for high performance. A possible change in ohmic loss in the electrochemical measurement must be taken into account an interface reaction may occur during electrode fabrication and cell operation.

4. Conclusions

The sintering temperature of a Ni-SDC cermet anode on a LSGM electrolyte is the key determinant of high performance. An anode sintered at a temperature higher than 1350°C could result in a substantial loss in performance. This loss appears to be caused mainly by the interface diffusion of nickel from the Ni-SDC anode to the LSGM electrolyte, although the grain-growth problem of Ni-SDC anode sintered at this temperature is also a contributing factor. In order to obtain a high performance Ni-SDC cermet anode, interface diffusion and severe grain growth must be avoided. For a Ni-SDC anode prepared from our SP composite powder on a LSGM electrolyte, it is recommended that the best sintering temperature is 1250°C based on a P_a value rather than a η_a value.

References

[1] T. Ishihara, H. Matsuda, Y. Tkita, J. Am. Chem. Soc. 116 (1994) 3801.
[2] T. Ishihara, H. Matsuda, Y. Tkita, Solid State Ionics 79 (1995) 147.
[3] T. Ishihara, M. Honda, T. Shibayama, H. Minami, H. Nishiquchi, Y. Takita, J. Electrochem. Soc. 145 (1998) 3177.
[4] M. Feng, J.B. Goodenough, K. Huang, C. Milliken, J. Power Sources 63 (1996) 47.
[5] K. Huang, R. Tichy, J.B. Goodenough, J. Am. Ceram. Soc. 81 (1998) 2565.
[6] K. Huang, M. Feng, J.B. Goodenough, J. Electrochem. Soc. 144 (1994) 3620.
[7] T. Ishihara, M. Honda, T. Shibayama, H. Minami, H. Nishiguchi, Y. Takita, J. Electrochem. Soc. 145 (1998) 3177.
[8] I. Yasuda, Y. Matsuzaki, K. Tsukamoto, T. Yamakawa, T. Koyama, 11th Fall Meeting of the Ceramic Society of Japan, Nagoya, Oct. 1–3, 1998, p. 201.
[9] M. Watanabe, H. Uchida, M. Shibata, N. Mochizuki, K. Amikura, J. Electrochem. Soc. 141 (1994) 342.
[10] K. Eguchi, J. Alloys Compd. 250 (1997) 486.
[11] K. Eguchi, T. Setoguchi, T. Inoue, H. Arai, Solid State Ionics 52 (1992) 165.
[12] H. Uchida, H. Suzuki, M. Watanabe, J. Electrochem. Soc. 145 (1998) 615.
[13] H. Uchida, H. Suzuki, M. Watanabe, J. Electrochem. Soc. 143 (1996) 1700.
[14] T. Takahasi, H. Iwahara, I. Ito, Denki Kagaku oyobi Kogyo Butsuri Kagaku 38 (1970) 509, Presently Electrochemistry.
[15] D.Y. Wang, D.S. Park, J. Griffith, A.S. Nowicki, Solid State Ionics 2 (1981) 95.
[16] R. Gerhardt, A.S. Nowicki, J. Am. Ceram. Soc. 69 (1986) 641.
[17] H. Yahiro, T. Ohuchi, K. Eguchi, J. Mater. Sci. 23 (1988) 1036.
[18] M. Mogensen, T. Lindegard, U.R. Hansen, G. Mogensen, J. Electrochem. Soc. 141 (1994) 2122.
[19] H. Yahiro, Y. Eguchi, K. Eguchi, H. Arai, J. Appl. Electrochem. 18 (1988) 527.
[20] M.J. Saeki, H. Uchida, M. Watanaba, Catal. Lett. 26 (1994) 149.
[21] M. Watanabe, H. Uchida, M. Yoshida, J. Electrochem. Soc. 144 (1997) 1739.
[22] K. Eguchi, T. Setoguchi, T. Inou, H. Arai, in: S.C. Singhal, H. Iwahara (Eds.), Solid Oxide Fuel Cells III, PV 93-4, The Electrochemical Society Proceedings Series, Pennington, NJ, 1993, p. 494.
[23] S. Matsukoka, T. Ikeguchi, S. Tamura, T. Setoguchi, K. Eguchi, H. Arai, Abstracts of the 58th Meeting of the Electrochemical Society of Japan, Noda, Chiba, Japan, 1991, p. 175.
[24] S. Ohara, T. Fukui, K. Mukai, K. Kodera, Y. Kubo, in: U. Stimming, S.C. Singhal, H. Tagawa, W. Lehnert (Eds.), Solid Oxide Fuel Cells V, PV 97-40, The Electrochemical Society Proceedings Series, Pennington, NJ, 1997, p. 815.
[25] T. Fukui, S. Ohara, K. Mukai, Electrochem. Solid-State Lett. 1 (1998) 120.
[26] T. Fukui, T. Obuchi, Y. Ikuhara, S. Ohara, K. Kodera, J. Am. Ceram. Soc. 80 (1997) 261.
[27] R. Marici, T. Fukui, S. Ohara, Y. Kubo, Presented at Processing and Properties of Advanced Engineering Materials Meeting, Toyohashi, Japan, Oct. 29–31, 1997.
[28] R. Marici, S. Ohara, T. Fukui, T. Inagaki, J. Fujita, Electrochem. Solid-State Lett. 1 (1998) 201.
[29] T. Kawada, N. Sakai, H. Yokokawa, M. Dokiya, M. Masashi, T. Itawa, J. Electrochem. Soc. 137 (1990) 3042.
[30] R.J. Aaberg, R. Tunold, R. Odegard, S. Tjelle, in: U. Stimming, S.C. Singhal, H. Tagawa, W. Lehnert (Eds.), Solid Oxide Fuel Cells V, Electrochemical Proceedings, Vol. 97-18, 1995, p. 557.
[31] S. Skaarup, B. Zachau-Christiansen, T. Jabobsen, High temperature electrochemistry: ceramics and metals, in: F.W. Poulsen, N. Bonanos, S. Linderoth, M. Mogensen, B. Zachau-Christiansen (Eds.), 17th Riso International Symposium on Metals Science, Roskilde, DK, 1996, p. 423.
[32] M. Watanabe, H. Uchida, M. Yoshida, J. Electrochem. Soc. 144 (1997) 1739.
[33] R. Maric, T. Fukui, S. Ohara, T. Inagaki, H. Yoshida, J. Fujita, K. Miura, Presented at the Conference of Sintering, SINTERING' 98, Belgrade, Yugoslavia, Sept. 1–4, 1998.